Experimental Physiology – *Modelling of Biological Systems*

Computational models of structure–function relationships in the pulmonary circulation and their validation

Merryn H. Tawhai[1], Kelly S. Burrowes[1] and Eric A. Hoffman[2]

[1] *Bioengineering Institute, University of Auckland, Private Bag 92019, Auckland, New Zealand*
[2] *Departments of Radiology and Biomedical Engineering, University of Iowa, Iowa City, IA 52242, USA*

The pulmonary airway, arterial, venous and capillary networks are vast complex branching and converging systems that are mechanically coupled to the surrounding lung tissue. Early studies that examined vascular or airway geometry relied on measurements from casts, but medical imaging now enables measurement of the lung *in vivo*, at controlled lung volumes. The high-quality data that imaging provides have prompted development of increasingly sophisticated models of the geometry of the airway and pulmonary vascular trees. The accurate spatial relationships between airway, vessel and tissue in these imaging-derived models are necessary for computational analysis that aims to elucidate regional airway–vessel–tissue interactions. Predictions of blood flow through multiscale imaging-derived models of the pulmonary arteries and capillary bed reveal geometry-dependent patterns of perfusion in response to gravity and lung orientation that cannot be predicted with simplified, summary representations of the pulmonary transport trees. Validation of such predictions against measures from functional imaging holds significant potential for explaining and differentiating normal and disease-related heterogeneity in regional blood flow calculated using perfusion imaging.

(Received 5 October 2005; accepted after revision 2 January 2006; first published online 11 January 2006)
Corresponding author M. H. Tawhai: Bioengineering Institute, University of Auckland, Private Bag 92019, Auckland, New Zealand. Email: m.tawhai@auckland.ac.nz

To accomplish respiratory gas exchange, the mammalian lung comprises several major transport systems – the pulmonary airways, arteries and veins – that function to bring air and blood into close contact at a vast surface for gas exchange. The airway system includes conducting airways that do not take part in respiratory gas exchange but can exchange highly soluble gases with the bronchial circulation and act to humidify air that enters the lung at less than body temperature and saturation with water vapour, and respiratory airways that have their 'walls' comprised of openings to pulmonary alveoli. The alveolar septa are covered in an extremely dense network of capillaries; the fragile barrier between alveolar gas and blood comprises a single layer of epithelial cells lining the alveoli, the interstitium which accommodates the connective tissue fibres and basement membranes, and a single layer of endothelial cells that form the major component of the capillary wall (Weibel, 1984).

The transport systems can be considered to be 'embedded' within the pulmonary parenchyma, or suspended in a vast fibre network as described by Weibel (1984). The fibre system initiates at the hilum and extends through the lung to the visceral pleura. The 'axial' fibre system begins at the main stem bronchus and progresses with the airways to the terminal bronchioles. The 'peripheral' fibre system is related to the visceral pleura and enwraps the lobar units. The pulmonary venous network follows the peripheral fibre system (between airways and arteries), while the arterial system follows the airways and therefore the axial fibre system. The axial fibre system continues into the respiratory tissue, encircling the entrances to the alveoli, and extending a fine fibre network over the alveolar septal surfaces and weaving through the capillary meshwork.

An accurate and detailed representation of geometry in computational models of anatomical structures is essential to deliver meaningful results from numerical simulations. Because the lungs are comprised of several mechanically and functionally coupled subsystems, computational models of the lung must vary in structure over a range of scales of interest. The model structure is also dependent on the problem to which it is applied: fluid-flow simulation requires three-dimensional meshes that accurately represent the complex surface airway

DOI: 10.1113/expphysiol.2005.030957

geometry (Lin & Hoffman, 2005), whereas inert-gas mixing (Verbanck & Paiva, 1990; Dutrieue *et al.* 2000) or airway thermodynamics (Tawhai & Hunter, 2004) can be modelled satisfactorily using conventional (in pulmonary physiology) one-dimensional trees with diameter information.

State-of-the-art medical imaging (specifically multidetector row computed tomography (MDCT) imaging for the air-filled lung tissue) provides high-resolution data from which subject-specific interdependent models of lung geometry can be constructed as computational domains through which a set of governing equations will be solved to simulate and understand function. By developing models on a subject-specific basis, the resulting computational meshes have spatially consistent relationships. The process of coupling functional models within the systems is therefore far more straightforward than for models developed independently from different data sets. A model with accurate spatial relationships between airway, vessel and the tissue to which they are tethered is a necessity for computational analysis of airway–vessel–tissue interactions such as coupling of ventilation distribution in 'embedded' airway models to the large deformation of the lung tissue (Tawhai *et al.* 2005, 2006).

Physically realistic model geometry

The geometry of the conducting airways. Airway model geometries have typically been constructed using measurements from painstaking morphometric studies such as Weibel (1963), Horsfield & Cumming (1968) or Phalen *et al.* (1978). Weibel's symmetric model A (Weibel, 1963) and Horsfield's asymmetric Δ model (Horsfield *et al.* 1971) are still widely used for computational studies because they summarize detailed anatomical data into idealized constructs that are relatively easy and computationally inexpensive to use.

In Weibel's symmetric model the mean length and diameter are presented for an average number of generations from the trachea to the terminal bronchioles, with each generation (N) having 2^N branches (where $N = 0$ for the trachea). The symmetric model enables representation of the vast conducting airway system by only 16 branches (one per generation), hence making it feasible to solve equations within a very small anatomically based description of the airway system.

The Horsfield Δ model is based upon the assumption that the airway tree bifurcates with a pattern of regular asymmetry defined by Δ, the difference in (Horsfield) order of two child branches. Horsfield *et al.* (1971) presented models with constant Δ through the majority of the conducting airway tree (the terminal airways require a slightly different pattern), and models with different Δ values in each lobe or bronchopulmonary segment. The model introduces a pattern of asymmetric branching and dimension asymmetry, but it does not include the spatial distribution of airways that is necessary for some computational studies.

Later anatomical studies, such as Krause *et al.* (1995) and Phillips & Kaye (1997), further analysed the geometry of the airway tree. The common limitation of these and previous anatomical studies is that measurements were made on relatively few excised airway or vascular casts, where the geometry of the measured structure might be quite different to that of the *in vivo* lung. This illustrates a major difference between anatomical studies of the lung and other body organs: under normal conditions the lung is far from its zero stress state, and its large elastic recoil means that excised tissue collapses when exposed to atmospheric pressure. Whereas a great deal of structural information can be gained by examining an excised muscular organ, the lung must be inflated or casts made of the conducting systems before the organ is in a suitable state for measurements. The upright human lung is known to deform in response to gravity, with tissue density highest in the gravitationally dependent region (that is, near the base of the lung as it rests against the diaphragm). Therefore cast measurements provide a 'snapshot' of the airway or vascular tree geometry under a uniform filling pressure that is generally higher than the normal pressures *in vivo*.

Advances in imaging technologies have provided a means to measure the lung geometry in its functioning state. Computed tomography (CT) studies have been carried out to measure relatively few *in vivo* airways (Sauret *et al.* 2002; Tawhai *et al.* 2004), and more extensive measurements have been made of single airway casts (Schmidt *et al.* 2004). As part of the development of the Human Lung Atlas (Hoffman *et al.* 2004), Saba *et al.* (2005) have presented an extensive analysis of human airway geometry at two volumes (functional residual capacity, FRC, the volume of the lung at rest prior to inspiration; and total lung capacity, TLC, the maximum volume of the lung) for 41 subjects based on imaging from MDCT. The analysis has demonstrated consistency between the geometry of the Human Lung Atlas airway tree at TLC and previous airway cast measures, CT measures, and a previous MDCT study of a single human airway tree (Tawhai *et al.* 2004). The extensive MDCT measures have identified a large decrease in the ratio of child-to-parent branch length from TLC to FRC, providing evidence that the more distal airways undergo a systematically larger increase in length during inspiration than the more central airways.

One challenge is to incorporate the increasing amount of imaging measures, such as those from the Human Lung Atlas, into computational models that can now feasibly be based on imaging for an individual. Tawhai *et al.* (2004) demonstrated how this can be achieved by developing

subject-specific models of the human and ovine lung and conducting airways. A volume-filling branching algorithm (Tawhai *et al.* 2000) was adapted to model the full extent of the conducting airway tree, such that the algorithm utilized the maximum amount of information from imaging data (airway and lung or lobe geometry from the Human Lung Atlas). The method fills an MDCT-defined finite element mesh of the lobes or lung (Fernandez *et al.* 2004) with an anatomically consistent airway tree that incorporates any imaged airways (currently as high as 10 branch divisions in humans and 23 in sheep) and has a branching geometry dependent on the shape of the host mesh. This method was shown to generate airway trees consistent with both the bifurcating geometry of the human lung (Fig. 1) and the monopodial branching pattern of the ovine lung. Consistent with the aim of integrating the maximum amount of information from imaging, the approach automatically incorporates additional geometric features of the lung as they are segmented. The approach marries techniques that were developed independently for model derivation (Tawhai *et al.* 2000; Fernandez *et al.* 2004) and segmented image analysis (Tschirren 2003) to produce subject-specific models of the lung that are unique in their ability to relate imaged structure to predicted function through computational simulations.

The use of subject-specific models is important for understanding how variation in individual branching or lung geometry impacts on the individual's distribution of ventilation (and therefore potentially their pattern of drug or pollutant transport), and whether there are subject groups that, owing to their lung geometry, are more susceptible to airway damage via inhaled substances, or to accelerated damage to their functional tissue because of different stress distributions. Subject-specific models also allow accurate comparison with regional functional imaging. For example, local wash-in and wash-out of xenon in an individual can be compared directly with regional model predictions.

The geometry of the pulmonary arterial and venous trees. To facilitate computational studies, the complexity of the pulmonary arterial and venous trees has previously been reduced by representing the tree as symmetric (Parker *et al.* 1997), as a self-similar fractal tree (Glenny & Robertson, 1991; Krenz *et al.* 1992; Bennett *et al.* 1996), or by representing an average flow path via summary morphometric parameters (Dawson *et al.* 1999). These models were developed to investigate the effects of large-scale alterations of branching geometry on haemodynamics in the lung, and therefore represent only the average geometry of the branching structure. They were designed for effective use in specific functional investigations, and did not aim to reflect the complex branching geometry of the pulmonary vascular trees accurately. However, these studies did all illustrate the large dependence of flow distribution on network geometry.

To model the pulmonary vascular trees in detail, Burrowes *et al.* (2005*a*) used an approach similar to that taken by Tawhai *et al.* (2004) to model the airway tree. The geometry of the largest pulmonary arterial and venous blood vessels was defined from segmentation of the same human subject's contrast-enhanced CT imaging (Burrowes *et al.* 2005*a*), and the non-segmented conventional arteries that accompany the airways were modelled using the volume-filling algorithm advanced by Tawhai *et al.* (2004). 'Conventional' or 'accompanying' vessels refers to the well-documented pattern of each airway being matched by an artery that follows the same approximate path, to supply the same region of tissue. In addition to the conventional arteries, the lung is known to contain many more 'supernumerary' vessels that diverge from a parent artery at close to 90 deg and branch rapidly to supply the closest respiratory tissue (Elliot & Reid, 1965). Because supernumerary vessels are not visible on angiograms and owing to the presence of a sphincter at their entrance, they are hypothesized to be unperfused under normal conditions (Elliot & Reid, 1965; Shaw *et al.* 1999), so it is not likely that they are visible on standard MDCT image reconstructions. The combined imaging and volume-filling branching algorithm can therefore generate a representation of the conventional accompanying blood vessels within the geometry of the lobes, but additional steps must be included to model the

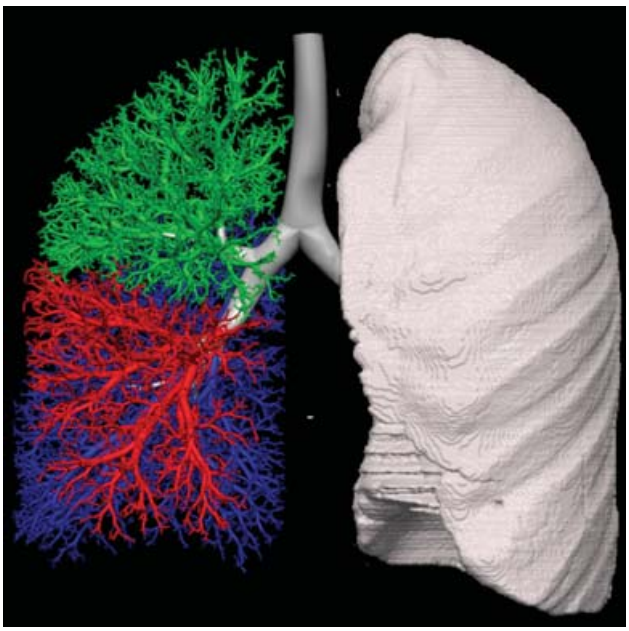

Figure 1. Volumetric imaging and finite element model of the airways
Volumetric reconstruction from MDCT imaging (left lung) and finite element model airways in the right upper lobe (green), right middle lobe (red), and right lower lobe (blue).

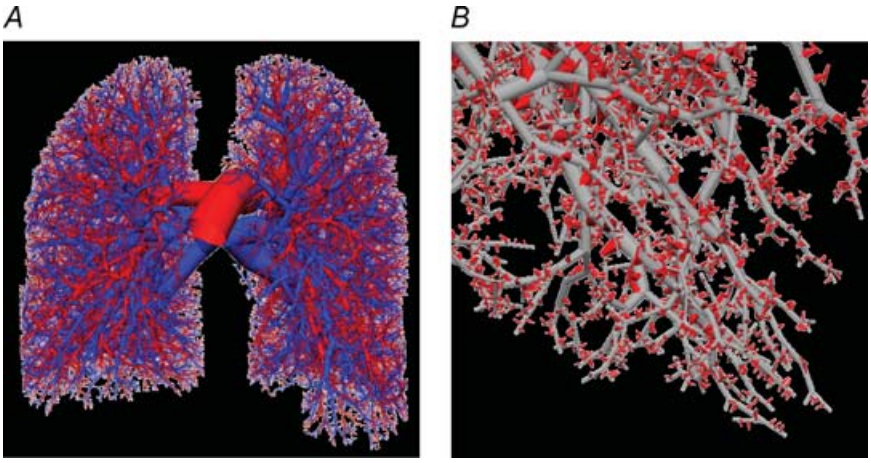

Figure 2. Detailed anatomically based model of the pulmonary arterial and venous trees
A, MDCT-based and volume-filling accompanying arteries (red) and veins (blue). *B*, supernumerary vessels (red) generated extending from the MDCT-algorithm-based model (from Burrowes *et al.* 2005*a*, with permission).

extensive system of supernumerary vessels. Burrowes *et al.* (2005*a*) modelled the supernumerary arteries and veins by assuming that they would arise from parent branches with diameter less than 1.5 mm (Weibel, 1963) at approximately 90 deg, and branch rapidly until they supplied the nearest pulmonary acini. One criterion that guided the model derivation was that the resulting tree should have Strahler branching ratios close to 3.0 (Horsfield, 1978) and 3.3 (Horsfield & Gordon, 1981) for the arterial and venous trees, respectively. Vessel diameters were defined as 0.3 of the parent diameter, and lengths were calculated using anatomical length-to-diameter ratios (Horsfield, 1978; Horsfield & Gordon, 1981). The vascular models, including supernumerary vessels, are illustrated in Fig. 2.

The geometry of the alveolar and capillary meshwork. The alveolar tissue has previously been modelled as a 3-D polyhedral network for mechanics studies (Denny & Schroter, 1996), and as a 3-D space-filling base structure for modelling the pulmonary microcirculation (Burrowes *et al.* 2004).

Burrowes *et al.* (2004) modelled a portion of the respiratory airways/alveolar tissue using a Voronoi meshing technique that creates a volume-filling polyhedral mesh of Voronoi 'cells' such that the resulting geometry is consistent with measured alveolated airway structure. In this approach (summarized in Fig. 3), a host volume is filled with space-filling model alveoli (one Voronoi cell = one alveolus) and central duct spaces to produce a 3-D mesh with anatomically consistent alveolar dimensions and surface-to-volume ratio. The technique exploits the geometric Delaunay–Voronoi relationship: a Delaunay triangulation has the property that for any set of triangulated points, the circle drawn through the triangle vertices (or sphere constructed through the tetrahedral vertices in 3-D) does not contain any other triangle vertex. A Voronoi tessellation is constructed by joining the circumcentres of adjacent Delaunay triangles (or tetrahedra).

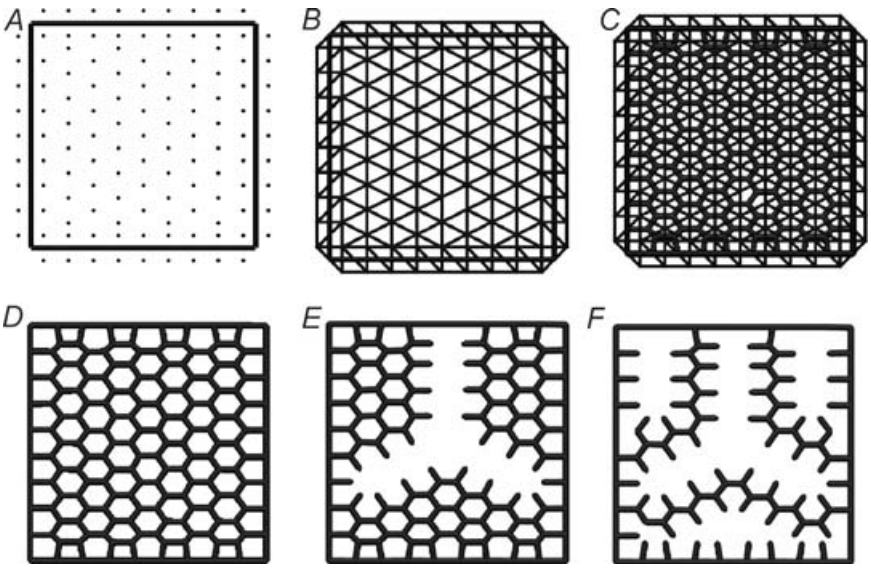

Figure 3. Generation of a model of the pulmonary alveolar tissue using a Voronoi–Delaunay meshing approach
A, host volume filled with a regular grid of points. *B*, Delaunay triangulation. *C*, Voronoi cells created to join the Delaunay triangle circumcentres. *D*, Voronoi tessellation. *E*, duct faces removed to aerate adjacent alveolar cells. *F*, final mesh has all cells as either duct or alveoli.

The Delaunay–Voronoi meshing technique provides a relatively simple way of creating alveolated airway structures within general host-volume shapes. The finite element meshes produced by the method are consistent with the mesh developed for mechanical analysis of the alveolar tissue by Denny & Schroter (1996). The mesh is continuous, space filling, and has an alveolar surface-to-volume ratio within 2.7% of the published value (Weibel, 1963).

The pulmonary capillaries form a dense sheet-like meshwork composed of short interconnected capillary segments. The capillaries are wrapped over the alveoli, with only a single sheet of capillaries between adjacent alveoli on the same alveolar duct. Because of the density of the capillary network, the classic model of the pulmonary microcirculation treats the capillary bed as a 'sheet' of blood bounded by two compliant layers of endothelium (Fung & Sobin, 1969). The sheet-flow model of alveolar blood flow simplifies the complex capillary geometry into a model that is appropriate for many computational studies of microcirculatory flow. However, the sheet-flow model cannot be used for investigating individual cell transit, segment blocking by neutrophils, or identification of preferential pathways for cell transit (Huang *et al.* 2001).

Discrete segmented models of the pulmonary microcirculation have been used by Huang *et al.* (2001), Dhadwal *et al.* (1997) and Burrowes *et al.* (2004) to investigate cellular transit. Dhadwal *et al.* (1997) modelled the capillaries on a single alveolar septum as a 6×6 square grid of interconnected segments. Huang *et al.* (2001) extended this model to generate a random orientation of the capillary segments, and connected six of the septae at opposite corners for simulation of red blood cell and neutrophil transit.

Burrowes *et al.* (2004) used a 2-D Delaunay–Voronoi meshing method to generate a segmented capillary mesh that wraps over the surface of model alveoli, with a single model capillary sheet between the adjacent alveoli. The method generates a capillary mesh to cover the 2-D alveolar septae of the volume-filling alveolar model previously described. The meshing technique (summarized in Fig. 4) can be applied not only to the fairly regular alveolar structure, but also to any irregular finite element representation of the alveoli. The resulting mesh has approximately 1000 capillary segments per alveolus, and 85 segments on average that a red blood cell would pass through as it traverses from a supplying arteriole to a draining venule.

Structure–function relationships in pulmonary perfusion

Experimental studies. Early studies of perfusion distribution in the human lung used relatively low-resolution external measures (e.g. West & Dollery, 1960; West *et al.* 1964; Bryan *et al.* 1964; Anthonisen & Milic-Emili, 1966) averaged over large regions of the lung. These studies typically measured a vertical gradient of reducing blood flow from the least (gravitationally) dependent to the most dependent regions of the lung, with the conclusion that hydrostatic pressure differences were the main determinant of blood flow distribution; this led to the well known zonal model of pulmonary blood flow. One of the predictions of the zonal model is that reversal of posture should result in reversal of the flow gradient. Advances in experimental techniques (Glenny *et al.* 1991) have provided higher resolution data. Such studies have suggested that gravity is only a minor determinant of pulmonary blood flow. Using microsphere injection measurements in baboons, Glenny *et al.* (1999) have demonstrated a persistent blood flow gradient with respect to position in the lung, somewhat independent of body posture, suggesting that there are additional mechanisms responsible for maintaining the

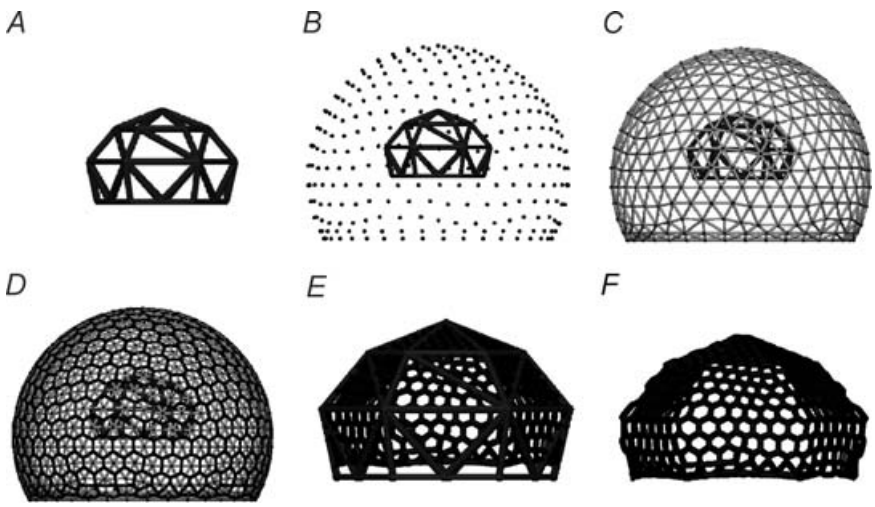

Figure 4. Generation of a continuous model of the pulmonary capillary network
A, a single alveolus. *B*, points generated over a portion of a unit sphere. *C*, 2-D Delaunay triangulation of sphere points. *D*, Voronoi tessellation for 2-D triangulation. *E*, Voronoi mesh projected onto the surface of the model alveolus. *F*, the final capillary mesh consists of the edges of the 2-D Voronoi cells.

flow gradient. A small amount of flow reversal was observed on inversion of posture, but not a complete reversal of the flow gradient as would be predicted by the zonal flow model. Other experimental studies of perfusion heterogeneity in different postures have agreed that factors other than gravity are largely responsible for flow distribution. Musch *et al.* (2002) used positron emission tomography (PET) imaging to assess the distribution of ventilation and perfusion in prone *versus* supine humans. They demonstrated that both ventilation and perfusion gradients (favouring caudal lung regions) were maintained in both postures. They also found that flow heterogeneity, as measured by the coefficient of variation squared, was unaffected by posture. Jones *et al.* (2001) produced similar results using electron beam computed tomography scans on healthy humans, also comparing perfusion distribution in the prone *versus* supine positions. Gravity was estimated to contribute only 22–34% of perfusion heterogeneity in the supine posture and 27–41% when subjects were prone.

The more recent imaging and experimental studies therefore conclude that gravitational gradients in flow exist, but that they are overwhelmed by other mechanisms. The relative contributions of gravity, vascular branching, hypoxic vasoconstriction and other unknown factors to pulmonary perfusion are still unclear, and remain under debate (West, 2002).

Computational modelling studies. In addition to direct experimental and imaging measures, pulmonary perfusion has been investigated using a variety of computational models (Glenny *et al.* 1991; Krenz *et al.* 1992; Parker *et al.* 1997; Dawson *et al.* 1999). Burrowes *et al.* (2004, 2005*b*) and Burrowes & Tawhai (2005) used physically realistic models of the segmented alveolar capillary bed and pulmonary arterial tree to examine the influence of gravity, asymmetric network branching and posture on perfusion. In the microcirculatory model, blood transport equations were solved within a realistic geometry exposed to pressure boundary conditions that were consistent with the West zonal theory of flow; in the arterial model simplified versions of the Navier–Stokes equations were solved within an elastic vessel network subjected to gravitational gradients in pleural and blood pressure.

Burrowes *et al.* (2004, 2005*b*) and Burrowes & Tawhai (2005) examined blood transit through the capillary bed and flow through the arterial tree as two separate systems (note that venous flow was not presented in these studies). This was necessary because of computational constraints: explicitly modelling each vessel in the full arterial, venous and capillary network was not possible. The models were therefore partitioned at a physiologically sensible level, and pressure boundary conditions for each model were set in a way that attempted to compensate for the lack of the full blood flow circuit.

Microcirculatory flow. At the microcirculatory level blood must be considered as a two-phase non-Newtonian fluid. Particles suspended in blood, particularly the red blood cells (RBCs), strongly influence the apparent viscosity of the blood and therefore the blood flow through the segmented network. The apparent viscosity of blood varies with vessel diameter, haematocrit (volume fraction of RBCs in blood) and blood cell velocity. In blood vessels smaller than approximately 300 μm in diameter, RBCs are preferentially distributed near the vessel centre (Secomb, 1995; Pries *et al.* 1996). The creation of a layer of zero haematocrit near the vessel wall reduces the apparent viscosity of blood in proportion to the decreasing vessel diameter, termed the Fahraeus–Lindqvist effect (Fahraeus & Lindqvist, 1931). Because the RBCs travel in the centre of the vessel their velocity is higher than that of plasma near the vessel wall, hence the tube haematocrit (haematocrit in the capillary segment) is reduced relative to the discharge haematocrit (haematocrit of blood entering or leaving). This dynamic reduction is known as the Fahraeus effect (Fahraeus, 1929). In addition to these two effects, RBCs are distributed disproportionately at bifurcations (phase separation) proportional to the relative flow rates in child vessels (Pries *et al.* 1990). To incorporate these effects into a simulation of microcirculatory blood flow, an iterative procedure is therefore used: pressure and flow are solved throughout the network assuming a using a Poiseuille-based flow equation and assuming an initially uniform haematocrit; the haemodynamics of the system are updated using empirical equations that account for the Fahraeus, Fahraues–Lindqvist and phase separation effects; and a dimensional model (Huang *et al.* 2001) is solved to update the capillary diameters. Burrowes *et al.* (2004) implemented the blood flow model presented by Huang *et al.* (2001) in a capillary geometry over the surface of a single alveolar sac. By exposing the model to arterial, venous and pleural pressures that increased linearly with descent down the vertical lung, they were able to demonstrate preferential pathways for blood cell transit, more homogeneous flow in the most gravitationally dependent regions, and large unrecruited regions of the capillary bed even in the tissue region of highest flow. The pattern of flow through the model was consistent with West's zonal theory for zones 2 and 3 (flow increasing in the direction of gravity, alveolar pressure < arteriole pressure). Zone 1 (zero flow, alveolar pressure > arteriole pressure) was not modelled, and zone 4 (decreasing flow in gravitationally dependent region) was not apparent because West's hypothesis that flow reduction occurs due to compression of extra-alveolar vessels was not incorporated into the model. Transit times through the model were generally faster than those measured

experimentally. This could be due to equal perfusion of the supplying arterioles in the model, whereas the arterioles that arise from supernumerary vessels would be likely to be unperfused.

Microcirculatory flow is difficult to quantify using imaging techniques; however, Won *et al.* (2003) have advanced a deconvolution–reconvolution method to determine regional pulmonary microvascular mean transit times (MTTs). The MTT measures from such an approach hold potential to provide a rich set of validation data for simulations of microcirculatory flow; conversely, the model flow predictions may provide guidance for parameterizing the analysis for calculation of MTT from the CT imaging.

Pulmonary arterial flow. To investigate the influence of normal arterial branching, gravity and posture, Burrowes *et al.* (2005*b*) and Burrowes & Tawhai (2005) solved a simplified version of the Navier–Stokes equations in elastic venous and arterial trees, subject to boundary conditions for pressures at the heart, pressures at the capillary bed, a gravitational acceleration vector and transpulmonary pressure. They demonstrated a persistent gradient of flow and flow heterogeneity in the absence of gravity (Fig. 5), and concluded that the long transit paths in the most apical and basal regions were the particular feature of the tree structure that caused a reduction of flow in these regions (Burrowes *et al.* 2005*b*). These predictions were consistent with measurements from high-resolution microsphere deposition studies (Glenny *et al.* 1999; Hlastala & Glenny, 1999), but by averaging the model results in thick 'slices' the prediction of an apparent gravitational flow gradient became more consistent with conclusions from the early, relatively low-resolution studies (West *et al.* 1964). That is, the mean pattern of flow in the upright lung model, with or without gravity, was similar to that measured by West *et al.* (1964) but attributed solely to gravity. Burrowes & Tawhai (2005) further extended the model to investigate incomplete reversal of flow upon reversal of body posture. Inversion of posture resulted in a clear effect on the gradient of pressure, and therefore radius, at all terminal vessels in the model. However, the effect on flow was less significant; while flow in the prone posture was consistently lower than flow supine, the flow at any terminal location was similar in either posture (Fig. 6). Because the arterial tree has regionally dependent path lengths (that is, longer branching paths to the most apical and basal regions) the resistance to flow in these model paths is similar regardless of posture, and therefore there is a persistent (non-gravitational) underlying pattern of flow in the model that is likely to exist in the real pulmonary arteries.

Future advances and validation with imaging

The two main limitations of the perfusion analyses of Burrowes and coworkers are that the capillary and arterial models were not coupled, and that neither system was exposed to realistic geometry changes as a result of tissue deformation. Coupling the arterial (and venous) and capillary models to simulate perfusion of the full pulmonary circuit will provide a better prediction of the relative effects of vascular branching and gravity. Because the vascular trees are 'embedded' within the lung lobes, coupling the model of blood flow to soft tissue deformation of the lung tissue will provide: (1) a realistic change in geometry of the vascular models when exposed to gravity or when changing volume; and (2) realistic pressures

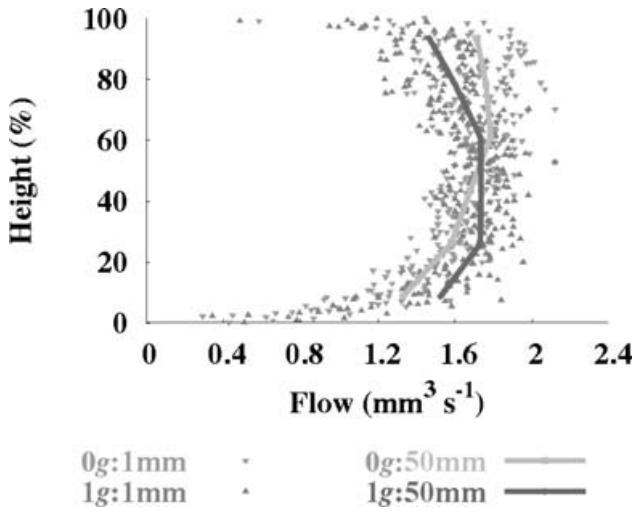

Figure 5. Blood flow at terminal pulmonary arterial locations (arterial vessels that accompany the terminal bronchioles) plotted against height in the vertical human lung, for zero gravity (0 *g*) and normal gravity (1 *g*)
Results are shown averaged in 1 mm slices and in 50 mm slices (from Burrowes *et al.* 2005*b*, with permission).

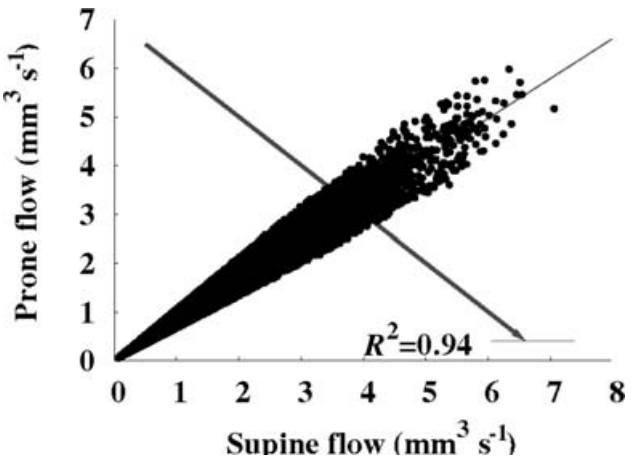

Figure 6. Blood flow at terminal pulmonary arterial locations in the prone posture plotted against flow in the supine posture at corresponding locations
The arrow indicates the predicted relationship if flow were to reverse fully with posture (from Burrowes & Tawhai 2005*c*, with permission).

acting on the vessels that result from expansion or recoil of the parenchymal tissue. Similar work to couple soft tissue mechanics and ventilation distribution has been presented by Tawhai *et al.* (2005, 2006).

The anatomically based models provide a uniquely controllable tool for probing the structure–function relationships that result in observed features of pulmonary perfusion. Current developments aim to link these computational predictions to functional measures by comparing subject-specific predictions of perfusion to MDCT measures of blood flow in the same subject. MDCT imaging can provide estimates of tissue density (to compare with the predicted soft tissue deformation) and of regional blood flow. One goal of this work is to understand the sensitivity of functional measures to changes in vascular geometry. This will provide a further set of functional parameters to populate the Human Lung Atlas.

References

Anthonisen NR & Milic-Emili J (1966). Distribution of pulmonary perfusion in erect man. *J Appl Physiol* **21**, 760–766.

Bennett SH, Goetzman BW, Milstein JM & Pannu JS (1996). Role of arterial design on pulse wave reflection in a fractal pulmonary network. *J Appl Physiol* **80**, 1033–1056.

Bryan AC, Bentivolgio LG, Beerel F, MacLeish H, Zidulka A & Bates DV (1964). Factors affecting regional distribution of ventilation and perfusion in the lung. *J Appl Physiol* **19**, 395–402.

Burrowes KS, Hunter PJ & Tawhai MH (2005*a*). Anatomically-based finite element models of the human pulmonary arterial and venous trees including supernumerary vessels. *J Appl Physiol* **99**, 731–738.

Burrowes KS, Hunter PJ & Tawhai MH (2005*b*). Evaluation of pulmonary arterial flow heterogeneity via an image-based computational model. *Acad Radiol* **12**, 1464–1474.

Burrowes KS & Tawhai MH (2005). Computational predictions of pulmonary blood flow gradients: gravity versus structure. *Respir Physiol Neurobiol* in press.

Burrowes KS, Tawhai MH & Hunter PJ (2004). Modeling RBC and neutrophil distribution through an anatomically based pulmonary capillary network. *Ann Biomed Eng* **32**, 585–595.

Dawson CA, Krenz GS, Karau KL, Haworth ST, Hanger CC & Linehan JH (1999). Structure-function relationships in the pulmonary arterial tree. *J Appl Physiol* **86**, 569–583.

Denny E & Schroter RC (1996). A mathematical model for the morphometry of the pulmonary acinus. *J Biomech Eng* **118**, 210–215.

Dhadwal A, Wiggs B, Doerschuk C & Kamm R (1997). Effects of anatomic variability of blood flow and pressure gradients in the pulmonary circulation. *J Appl Physiol* **83**, 1711–1720.

Dutrieue B, Vanholsbeeck F, Verbanck S & Paiva M (2000). A human acinar structure for simulation of realistic alveolar plateau slopes. *J Appl Physiol* **89**, 1859–1867.

Elliot FM & Reid L (1965). Some new facts about the pulmonary artery and its branching pattern. *Clin Radiol* **16**, 193–198.

Fahraeus R (1929). The suspension stability of blood. *Physiol Rev* **9**, 241–274.

Fahraeus R & Lindqvist T (1931). The viscosity of the blood in narrow capillary tubes. *J Appl Physiol* **96**, 562–568.

Fernandez J, Mithrartne P, Thrupp S, Tawhai MH & Hunter PJ (2004). Anatomically based geometric modelling of the musculo-skeletal system and other organs. *Biomech Model Mechanobiol* **2**, 139–155.

Fung YC & Sobin SS (1969). Theory of sheet flow in lung alveoli. *J Appl Physiol* **26**, 472–488.

Glenny RW, Bernard S, Robertson HT & Hlastala MP (1999). Gravity is an important but secondary determinant of regional pulmonary blood flow in upright primates. *J Appl Physiol* **86**, 623–632.

Glenny RW, Polissar L & Robertson HT (1991). Relative contribution of gravity to pulmonary perfusion heterogeneity. *J Appl Physiol* **71**, 2449–2452.

Glenny RW & Robertson HT (1991). Fractal modelling of pulmonary blood flow heterogeneity. *J Appl Physiol* **70**, 1024–1030.

Hlastala MP & Glenny RW (1999). Vascular structure determines pulmonary blood flow distribution. *News Physiol Sci* **14**, 182–186.

Hoffman EA, Clough AV, Lin C-L, McLennan G, Reinhardt JM, Simon BA, Sonka M, Tawhai MH, Van Beek EJ & Wang G (2004). The comprehensive imaging-based analysis of the lung: a forum for team science. *Acad Radiol* **11**, 1370–1380.

Horsfield K (1978). Morphometry of the small pulmonary arteries in man. *Circ Res* **42**, 593–537.

Horsfield K & Cumming G (1968). Morphology of the bronchial tree in man. *J Appl Physiol* **24**, 373–383.

Horsfield K, Dart G, Olsen DE, Filley GF & Cumming G (1971). Models of the human bronchial tree. *J Appl Physiol* **31**, 207–217.

Horsfield K & Gordon I (1981). Morphometry of pulmonary veins in man. *Lung* **159**, 211–218.

Huang Y, Doerschuk C & Kamm R (2001). Computational modeling of RBC and neutrophil transit through the pulmonary capillaries. *J Appl Physiol* **90**, 545–564.

Jones AT, Hansell DM & Evans TW (2001). Pulmonary perfusion in supine and prone postures: an electron beam study. *J Appl Physiol* **76**, 882–892.

Krause E, Bandt C, Schulz A & Schulz H (1995). Fractal exponents for the upper airways of mammalian lungs. *Statist Software Newsletter* **20**, 583–590.

Krenz GS, Linehan JH & Dawson CA (1992). A fractal continuum model of the pulmonary arterial tree. *J Appl Physiol* **72** (6), 2225–2237.

Lin C-L & Hoffman EA (2005). A numerical study of gas transport in human lung models. *Proc SPIE* **5746**, 92–100.

Musch G, Layfield JDH, Harris RS, Melo MFV, Winkler T, Callahan RJ, Fischman AJ & Venegas JG (2002). Topographical distribution of pulmonary perfusion and ventilation, assessed by PET in supine and prone humans. *J Appl Physiol* **93**, 1841–1851.

Parker JC, Cave CB, Ardell JL, Hamm CR & Williams SG (1997). Vascular tree structure affects lung blood flow heterogeneity simulated in three dimensions. *J Appl Physiol* **93**, 1370–1382.

Phalen RF, Yeh HC, Schum GM & Raabe OG (1978). Application of an idealized model to morphometry of the mammalian tracheobronchial tree. *Anat Rec* **190**, 167–176.

Phillips CG & Kaye SR (1997). On the asymmetry of bifurcations in the bronchial tree. *Resp Physiol* **107**, 85–98.

Pries AR, Secomb TW & Gaehtgens P (1996). Biophysical aspects of blood flow in the microvasculature. *Cardiovascular Res* **32**, 654–667.

Pries AR, Secomb TW, Gaehtgens P & Gross JF (1990). Blood flow in microvascular networks – experiments and simulation. *Circ Res* **67**, 826–834.

Saba OI, Delsing A, Sieren JP, Nixon E, Tschirren J, McLennan G & Hoffman EA (2005). Normative airway geometry and topology measured by multidetector-row CT (MDCT) at two lung volumes. *Proceedings of the Am Thorac Soc* **2**, A333 (Abstract Issue).

Sauret V, Halson PM, Brown IW, Fleming JS & Bailey AG (2002). Study of the three-dimensional geometry of the central conducting airways in man using computed tomographic (CT) images. *J Anat* **200**, 123–134.

Schmidt A, Zidowitz S, Kriete A, Denhard T, Krass S & Pietgen H (2004). A digital reference model of the human bronchial tree. *Comput med Imaging Graph* **28**, 203–211.

Secomb TW (1995). Mechanics of blood flow in the microcirculation. *Biol Fluid Dynamics* **49**, 305–321.

Shaw AM, Bunton DC, Fisher A, McGrath JC, Montgomery I, Daly C & MacDonald A (1999). V-shaped cushion at the origin of bovine supernumerary arteries: structure and putative function. *J Appl Physiol* **87**, 2348–2356.

Tawhai MH & Hunter PJ (2004). Modeling water vapor and heat transfer in the normal and the intubated airway. *Ann Biomed Eng* **32**, 609–622.

Tawhai MH, Hunter PJ, Tschirren J, Reinhardt JM, McLennan G & Hoffman EA (2004). CT-based geometry analysis and finite element models of the human and ovine bronchial tree. *J Appl Physiol* **97**, 2310–2321.

Tawhai MH, Nash MP & Hoffman EA (2006). An imaging-based computational approach to model ventilation distribution and soft tissue deformation in the ovine lung. *Acad Radiol* **13**, 113–120.

Tawhai MH, Nash MP, Tschirren J, Hoffman EA & Hunter PJ (2005). An image-based computational model of ovine lung mechanics and ventilation distribution. *Proc SPIE* **5746**, 84–91.

Tawhai MH, Pullan AJ & Hunter PJ (2000). Generation of an anatomically based three-dimensional model of the conducting airways. *Ann Biomed Eng* **28**, 793–802.

Tschirren J (2003). Segmentation, anatomical labeling, branchpoint matching, and quantitative analysis of human airway trees in volumetric CT images. PhD Thesis, University of Iowa, Iowa City, IA, USA.

Verbanck S & Paiva M (1990). Model simulations of gas mixing and ventilation distribution in the human lung. *J Appl Physiol* **69**, 2269–2279.

Weibel ER (1963). *Morphometry of the Human Lung*. Springer-Verlag, Berlin.

Weibel ER (1984). *The Pathway for Oxygen – Structure and Function of the Mammalian Respiratory System*. Harvard University Press, Cambridge, MA, USA.

West JB (2002). Comment on: Importance of gravity in determining the distribution of pulmonary blood flow (*J Appl Physiol* **92**, 745–762). *J Appl Physiol* **93**, 1888–1889; author reply 1889–1891.

West JB & Dollery CT (1960). Distribution of blood flow and ventilation-perfusion ratio in the lung, measured with radioactive CO_2. *J Appl Physiol* **15**, 405–410.

West JB, Dollery CT & Naimark A (1964). Distribution of blood flow in isolated lung: relation to vascular and alveolar pressures. *J Appl Physiol* **19**, 713–724.

Won C, Chon D, Tajik J, Tran BQ, Robinswood GB, Beck KC & Hoffman EA (2003). CT-based assessment of regional pulmonary microvascular blood flow parameters. *J Appl Physiol* **94**, 2483–2493.

Acknowledgements

The authors would like to acknowledge the financial support of the Woolf Fisher Trust (Maurice Paykel Post Doctoral Fellowship), the Royal Society of New Zealand Marsden Grant 01-UOA-070 MIS, and the National Institutes of Health through grant no. HL064368.